受入
97-27-116
高工研図書室

KEK Preprint 97-116
August 1997
H

High-Precision Magnetic Field Mapping with a Three-dimensional Hall Probe for a T-violation Experiment in $K_{\mu 3}$ Decay

T. IKEDA, M.D. CHAPMAN, Y. IGARASHI, J. IMAZATO, J.M. LEE,
M.M. KHABIBULLIN, O.V. MINEEV, H.M. SHIMIZU, S. SHIMIZU, A. SUZUKI,
A. WATANABE and T.K. YOKOI

Submitted to Nucl Instrum. Meth.

* *From April 1, 1997,* ***High Energy Accelerator Research Organization (KEK)*** *was newly established. The new organization is restructured of three reseach institutes, National Laboratory for High Energy Physics (KEK), Institues of Nuclear Study (INS), Univ. of Tokyo and Meson Science Laboratory, Faculty of Science, Univ. of Tokyo.*

High Energy Accelerator Research Organization (KEK), 1997

KEK Reports are available from:

Information Resources Division
High Energy Accelerator Research Organization (KEK)
1-1 Oho, Tsukuba-shi
Ibaraki-ken, 305
JAPAN

Phone: 0298-64-5137
Fax: 0298-64-4604
Cable: KEK OHO
E-mail: Library@kekvax.kek.jp (Internet Address)
Internet: http://www.kek.jp

High-Precision Magnetic Field Mapping with a Three-dimensional Hall Probe for a T-violation Experiment in $K_{\mu 3}$ Decay

Tokihiro Ikeda[a], Michael D.Chapman[b], Youichi Igarashi[a], Jun Imazato[b], Jong Man Lee[c,1], Marat M.Khabibullin[d], Oleg V.Mineev[d], H.M.Shimizu[b,2], Suguru Shimizu[e,3], Atsushi Suzuki[a,4], Akifumi Watanabe[a], T.K.Yokoi[f]

[a] *Institute of Physics, University of Tsukuba, Tsukuba-shi, Ibaraki-ken, 305 Japan*

[b] *High Energy Accelerator Research Organization (KEK), Tsukuba-shi, Ibaraki-ken, 305 Japan*

[c] *Yonsei University, 134 Shinchon-dong Seoul, 120-749, Korea*

[d] *Institute for Nuclear Research, Russian Academy of Sciences, 117312 Moscow, Russia*

[e] *Department of Applied Physics, Tokyo Institute of Technology, Meguro-ku, Tokyo, 152 Japan*

[f] *Faculty of Science, University of Tokyo, Bunkyo-ku, Tokyo, 113 Japan*

Abstract

High-precision magnetic-field mapping was performed for an experiment to search for a violation of time-reversal invariance in the $K^+ \to \pi^0 \mu^+ \nu_\mu$ decay at the KEK proton synchrotron. A commercially available three-dimensional Hall probe was used in conjunction with a specially designed mapping device and a goniometer system. Details concerning the measurement principle, calibration, actual measurements and analysis are described.

[1] Present address: Korea Research Institute of Standards and Science Yuseong-Gu, Taejon 305-340, Korea

[2] Present address: Institute of Physical and Chemical Research, 2-1 Hirosawa, Wako, Saitama 351-01, Japan

[3] Present address: Department of Physics, Faculty of Science, Osaka University, Toyonaka, Osaka, 560 Japan

[4] Present address: HITACHI Medico, 2-1 Shintoyofuta, Kashiwa, Chiba, 277 Japan

1 Introduction

1.1 Measurement of transverse polarization in the E246 experiment

The E246 collaboration is aiming to search for a violation of time-reversal invariance in the $K^+ \to \pi^0 \mu^+ \nu_\mu$ decay ($K_{\mu 3}$) at the KEK proton synchrotron. In this experiment the transverse polarization (P_T) of muons, which is the component of polarization normal to the decay plane, is precisely measured. P_T can be expressed as a vector triple correlation,

$$P_T = \frac{\vec{s_\mu} \cdot (\vec{p_\pi} \times \vec{p_\mu})}{|\vec{p_\pi} \times \vec{p_\mu}|},$$

where $\vec{s_\mu}$ is the spin vector of a muon and $\vec{p_\pi}$ and $\vec{p_\mu}$ are momentum vectors of a muon and pion, respectively. Since P_T is odd under time-reversal, a non-zero value of this observable signals T-violation. The most important feature of the $K_{\mu 3}$ muon transverse polarization is the fact that there is no contribution from the standard model through the Kobayashi-Maskawa scheme. Therefore, we might be able to search for additional or alternative sources of CP-violation beyond the standard model, based on its extension or on the introduction of new interactions. This experiment will achieve a limit of $\Delta P_T \sim 10^{-3}$, which corresponds to the limit of Δ Im $\xi \sim 6 \times 10^{-3}$. [1]

The E246 experiment employs the Superconducting Toroidal Spectrometer located at the low-momentum beam channel K5 at the KEK-PS. Stopped kaons are used in this experiment. A schematic view of the experimental setup is shown in Fig.1. A kaon beam of 660 MeV/c momentum is selected by a Fitch-type Cherenkov counter, slowed down by a momentum degrader and then stopped in an active target made of a bundle of scintillating fibers and located at the center of the magnet. The decay μ^+ from the $K_{\mu 3}$ in the target is momentum-analyzed by one of the 12 magnet gaps and stopped in a polarimeter in which the decay positron asymmetry is measured to deduce P_T. The momentum vector of π^0 is determined by a π^0 detector, which comprises 768 CsI (Tl) crystals. The π^0 direction is reconstructed from the energies and directions of the two gamma rays of $\pi^0 \to 2\gamma$ decay.

The transverse polarization of muons is determined by the polarimeter, which is located at the exit of a gap (Fig.2). A muon stops and decays in muon stoppers made of a stack of 99.99% pure aluminum plates. A positron from the decay of $\mu^+ \to e^+ \nu_e \bar{\nu_\mu}$ is emitted with the following angular and time distribution:

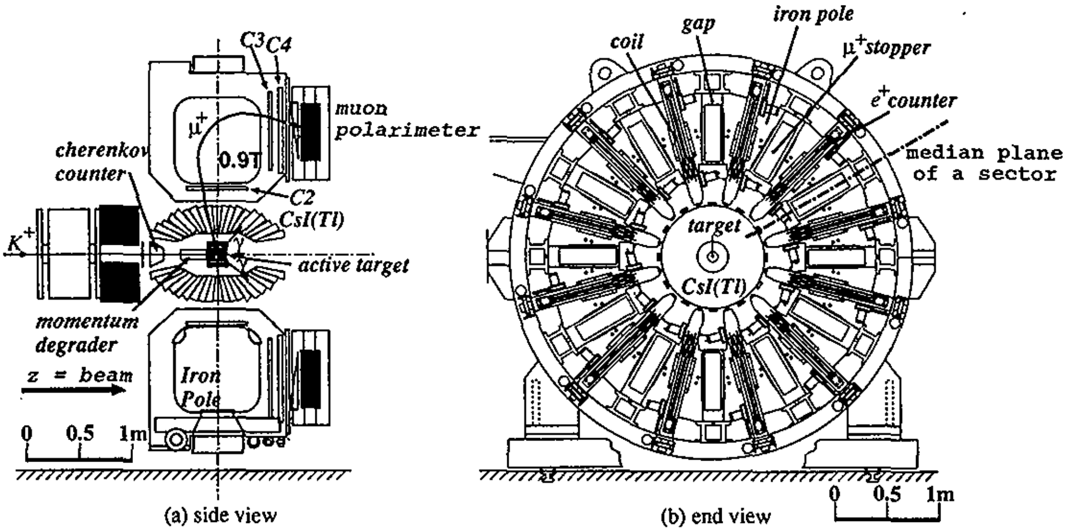

Fig. 1. **E246 setup:** (a) A kaon beam of momentum 660 MeV/c is selected by a Fitch-type Cherenkov counter, slowed down by a momentum degrader and then stopped in an active target located at the center of the magnet. The decay μ^+ from the $K_{\mu 3}$ is momentum-analyzed by one of the 12 magnet gaps under the excitation of 0.9 T and stopped in a polarimeter. C2, C3 and C4 are multi-wire proportional chambers for tracking. (b) End view of the magnet: It has 12 identical gaps with perfect 30 degree rotational symmetry. A positron counter is located at the middle of two stoppers.

$$f(\theta, t) = N_0 \, \mathrm{e}^{-\lambda t} \left\{ 1 + \frac{1}{3} P_\mu \cos\theta \right\},$$

where the decay constant (λ) is $1/2.2\ \mu\mathrm{s}^{-1}$ and θ is the positron emission angle relative to the muon spin direction. It means that the positron tends to be emitted in the same direction as the muon spin. Our interest is in measuring a possible tiny transverse component of the polarization in the presence of large T-conserving polarization components. The counters for detecting the decay positrons are located at both sides of the median plane, as shown in Fig.2. With this setup, P_T is extracted as

$$P_T = \frac{1}{\alpha} \cdot \frac{N_L - N_R}{N_L + N_R},$$

where N_L, N_R are the counts in the positron counters on the left- and right-hand sides, respectively. The analyzing power α incorporates the precession of muon spin vector around the magnetic-field vector. The field for this muon spin rotation (μSR) is essentially a fringing field of the toroidal magnet, and it was designed to be symmetrical across the median plane in order to make this

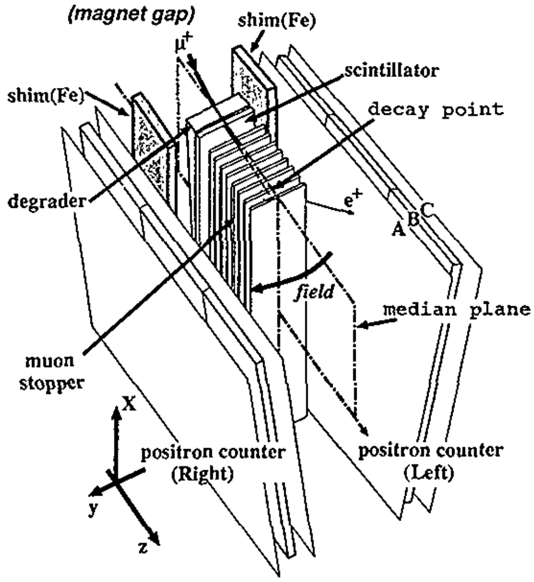

Fig. 2. **Schematic structure of the muon polarimeter**: The transverse polarization of muons, which should be directed normal to the median plane, is determined by the polarimeter. A muon stops and decays in the muon stopper. The positron tends to be emitted in the same direction as the muon spin. The positron counters are located at both sides of the median plane. The signal from the scintillator behind the degrader is regarded as μ^+ enters the polarimeter. A positron is detected as a triple-coincidence of three scintillators of A, B and C.

method valid. Fig.3 shows the flux distribution of the inhomogeneous field on the stopper, together with magnet yoke and iron shims.

The symmetry of the field distribution is also essential from the following consideration. In $K_{\mu 3}$ decay, the polarization component lying in the decay plane (in-plane component) is almost unity. Due to precession, the in-plane component can be oriented to a positron counter, namely the P_T direction. However, the spurious effect from this rotation can be cancelled out after integration over the decay time and over the stopper volume, as long as the symmetry of the muon-stopping distribution and the symmetry of the field distribution across the median plane are assured. The symmetry of the muon-stopping distribution can be ensured from the tracking of muons with multi-wire proportional chambers. The field symmetry at an excitation of B = 0.9 T is primarily determined by the yoke alignment. Also, trimming plates were installed to guarantee the symmetry of the field including the contribution from coils. These plates are made of pure Fe with high permeability and positioned accurately relative to the yoke, as shown in Figs.2 and 3.

The depolarization due to some impurity in aluminum muon stoppers was

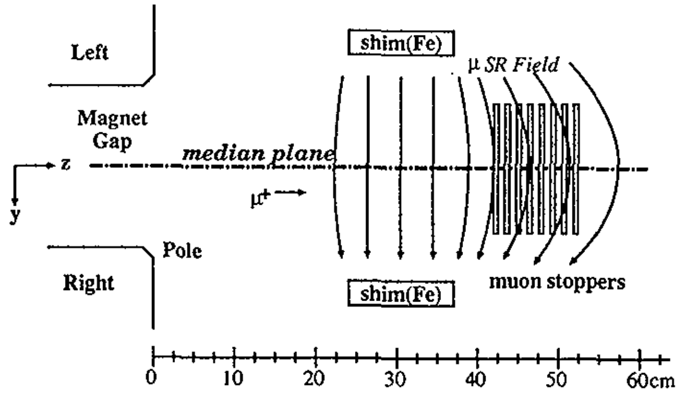

Fig. 3. **Flux distribution on the stopper with poles and shims:** The field for μSR was designed to be symmetrical across the median plane. The flux distribution is inhomogeneous. The field is primarily determined by the pole alignment, which is good enough; however, in order to guarantee the symmetry of the field including the contribution from coils, trimming plates (shims) were installed.

checked by a μSR experiment with fully polarized muons at the meson science laboratory of University of Tokyo. No relaxation of the polarization was detected in our stopper with a purity of 99.99% aluminum. The performance of each detector was described in an earlier report [2].

1.2 Requirements for the field distribution and field mapping

The asymmetry of μSR field flux distribution might cause a systematic error in the P_T measurement. The earth field and the field flux from unexpected magnetized materials around the polarimeter might induce an asymmetric field. These stray fields are on the level of 0.1 Gauss. Since the μSR field, itself, has a strength in the range between 100 and 300 Gauss on the muon stopper, the stray field makes a relatively negligible perturbation. However, high-precision field mapping was necessary for confirming the symmetry of the real μSR field and for estimating any systematic error due to the field structure. Taking into account the stopping distribution of muons, it was determined that field measurements with an accuracy of 0.5 mm for position, 0.5 Gauss for the field component and better than 10^{-2} radian for a coordinate determination were warranted. To attain these precisions, the following items were required.

(i) **High-precision positioning of a measured point:**
  - The limit in the accuracy of a measurement device assembly is about 0.1 mm.

- An installation method of the device to the toroidal magnet should be developed by considering the various effects of gravitation at 12 different orientations.

(ii) **Mechanism of the measurement to guarantee the symmetry with respect to the median plane**

(iii) **Accurate measurement of the three field components**

(iv) **High-speed measurements.**

As for the last item, the mapping was to be completed before installing other detector elements. It was necessary to finish the measurements in a short time.

1.3 Problems with Hall-probe measurements

In the present case, a Hall probe is the best tool, because the μSR field has an inhomogeneous structure and accurate positioning is required. The Hall-probe method has been applied for a number of field mappings in high-energy particle and nuclear-physics experiments [3–6]. However, this method has some limitations. The output voltage of a Hall probe (V_H) has a temperature dependence. In real use, the room temperature has to be monitored or carefully controlled. The Hall voltage (V_H) has non-linear terms to the field. One is a residual voltage under zero field; another is the planar Hall effect, which is proportional to the square of the field and has an angular dependence. Therefore, careful calibrations to determine these non-linear terms is required. As for positioning and alignment of the probe, there is some ambiguity in locating the exact center point and in determining the angles of the Hall plane relative to the probe. Especially, for a three-dimensional (3D) measurement with three individual Hall elements, precise simultaneous determinations of orientation and position are essential.

In order to satisfy the requirements and to overcome the problems mentioned above, the following advanced techniques were employed:

(i) **3D Hall probe on a goniometer:** A 3D Hall probe, (BH-703 , F.W.Bell) with three elements embedded in it was installed in a goniometer head. The head can be rotated in any direction around three orthogonal axes. This rotation capability was valuable for a precise extraction of linear as well as non-linear term of the field component (see section 2).

(ii) **3D device of high performance:** We developed a 3D scanning device, in which the goniometer was mounted. The goniometer on the base plate can move in three dimensions to any point by computer control with an accuracy of 0.1 mm. The alignment of the 3D device employed a laser positioning system.

(iii) **Accurate temperature measurement:** For temperature monitoring, three thermocouples were installed on the 3D Hall probe in the Hall-probe box. Also the room temperature was kept constant by an airconditioner.

(iv) **Careful calibration**: In order to determine the position accurately, the three elements in the mould were fixed precisely. To fix any misalignment in the orientation of each element and to understand the linear and non-linear terms in V_H, the calibration was done in a homogeneous field of 1.0 T with a general-purpose dipole magnet.

The principle and advantages of field mapping using the goniometer is described in section 2, and the details of the 3D device and the goniometer system are given in section 3. The actual procedure of the probe calibration, the measurement and analysis are presented in sections 4 and 5, respectively.

2 High-Precision Field Measurement with Hall Elements

The probe output (V_H) from the normal Hall effect is proportional to the field component normal to the element plane. It is measured as the induced voltage of the two sides of the Hall current direction ($\vec{I}$), as shown in Fig.4. The vector, $\vec{n}$, is the normal vector to the plane. $\vec{B}$ is the magnetic field vector

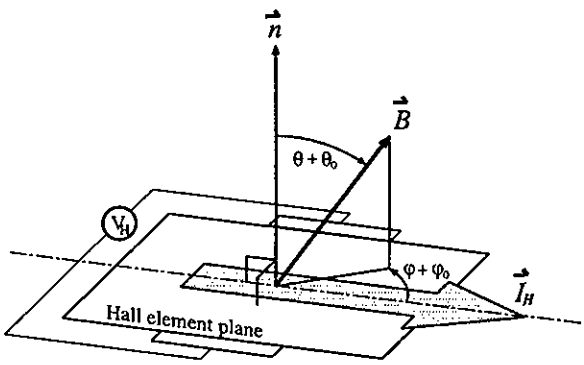

Fig. 4. **Definition of the angles:** $\vec{I}_H$ is the direction of the Hall current on a Hall element plane. The vector, $\vec{n}$, is the normal vector to the plane. $\vec{B}$ is the magnetic field vector at the point. V_H is measured as an induced voltage between the both sides of the Hall current. θ_0, ϕ_0 are the offsets of the element angles including the mis-alignment of the plane.

at the point. For higher fields, V_H shows a non-linear term due to the field component parallel to the element plane, as mentioned before, i.e., the planar Hall effect. Taking these effects into account, the Hall probe output (V_H) is expressed as

$$V_H = V_0 + GB\cos(\theta + \theta_0) + PB^2 \sin^2(\theta + \theta_0)\sin 2(\phi + \phi_0), \quad (1)$$

where V_0 is the residual voltage at zero field, the second term is the normal Hall effect with G being the Hall coefficient, including the Hall current ($G = I_H \cdot c$), and B is the field value; the third term is the planar Hall effect with P being the planar Hall coefficient. The angles (θ, ϕ) are the polar and azimuthal angles of the field vector, as shown in Fig.4. The 3D probe (a commercial unit) has an advantage in practical field mapping in view of (1) compactness of the probe and (2) time saving of the mapping; three field components can be measured simultaneously in one scan. Ideally, each Hall element (e.g., x-element) should be perpendicular to other two elements (e.g., y- and z-elements). However, there may be a misalignment of the orientation. θ_0, ϕ_0 are the offsets of the element angles, including these misalignments, which should be experimentally determined. Moreover, if the three elements are embedded in a mould and cannot be seen from outside, the positioning of the element centers and the above-mentioned determination of the offset angles become more complicated and tedious. In the present work we introduced a new method using a small goniometer head to overcome these problems. The probe mounted on the goniometer has not only the ease of angular adjustment, but also provides us with the ability to perform a measurement with the configuration of a flipped or 90°-rotated element. The former is of course important in transferring an angular system from the calibration to the mapping. Also, the latter enables us:

(i) to extract the normal Hall effect, eliminating the influence of the planar Hall term, and
(ii) to perform rationalized mapping, which guarantees the exact symmetry of the measurement under the condition of a small Hall planar effect.

In the following, these points are discussed in some detail. The Eulerian angles are defined as the relation between two orthogonal coordinate systems shown in Fig.5. We introduce the Hall probe frame (ξ, η, ζ) on which a Hall element is fixed, and laboratory frame (x, y, z) which represents the coordinate of mapping and a field vector. These are related by an Eulerian transformation:

$$\begin{pmatrix} x \\ y \\ z \end{pmatrix} = A \begin{pmatrix} \xi \\ \eta \\ \zeta \end{pmatrix},$$

where A is a matrix ;

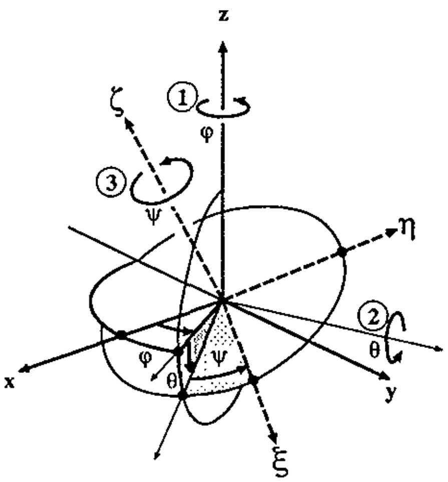

Fig. 5. **Definition of the Eulerian angles**: The Hall-element frame (ξ, η, ζ), and laboratory frame (x, y, z), which represents the coordinate of mapping and the field vector.

$$A = \begin{pmatrix} \cos\psi & \sin\psi & 0 \\ -\sin\psi & \cos\psi & 0 \\ 0 & 0 & 1 \end{pmatrix} \begin{pmatrix} \cos\theta & 0 & -\sin\theta \\ 0 & 1 & 0 \\ \sin\theta & 0 & \cos\theta \end{pmatrix} \begin{pmatrix} \cos\phi & \sin\phi & 0 \\ -\sin\phi & \cos\phi & 0 \\ 0 & 0 & 1 \end{pmatrix}$$
$$= \begin{pmatrix} a_{11} & a_{12} & a_{13} \\ a_{21} & a_{22} & a_{23} \\ a_{31} & a_{32} & a_{33} \end{pmatrix}.$$

The Eulerian angles (ϕ, θ and ψ) are defined in Fig.5. The matrix elements a_{ij} $(i, j = 1, 3)$ can be calculated as follows:

$$\begin{aligned}
a_{11} &= \cos\psi\cos\phi\cos\theta - \sin\psi\sin\phi, \\
a_{21} &= -\sin\psi\cos\phi\cos\theta - \cos\psi\sin\phi, \\
a_{31} &= \cos\phi\sin\theta, \\
a_{12} &= \cos\psi\sin\phi\cos\theta + \sin\psi\cos\phi, \\
a_{22} &= -\sin\psi\sin\phi\cos\theta + \cos\psi\cos\phi, \\
a_{32} &= \sin\phi\sin\theta, \\
a_{13} &= -\cos\psi\sin\theta, \\
a_{23} &= \sin\psi\sin\theta, \\
a_{33} &= \cos\theta.
\end{aligned}$$

Below, the main features of the goniometer method are described using the Eulerian angles of the element.

We now look at the z-element, whose normal vector ($\vec{n}$) and current vector ($\vec{I}$) are fixed to the ζ and ξ axes, respectively. They can be expressed in the laboratory frame as

$$\vec{n}_{Lab} = A \begin{pmatrix} 0 \\ 0 \\ 1 \end{pmatrix} = \begin{pmatrix} a_{13} \\ a_{23} \\ a_{33} \end{pmatrix}, \qquad \vec{I}_{Lab} = A \cdot I \begin{pmatrix} 1 \\ 0 \\ 0 \end{pmatrix} = I \begin{pmatrix} a_{11} \\ a_{21} \\ a_{31} \end{pmatrix}.$$

The Hall voltage can be expressed as:

$$\begin{aligned} V_H =& g \;\; \vec{n}_{Lab} \cdot (\vec{B} \times \vec{I}_{Lab}) + V_{PH} \\ =& g \;\; (a_{13}, a_{23}, a_{33}) \begin{pmatrix} a_{21}B_z - a_{31}B_y \\ a_{31}B_x - a_{11}B_z \\ a_{11}B_y - a_{21}B_x \end{pmatrix} + V_{PH} \\ =& g \,\{a_{12}(a_{21}B_z - a_{31}B_y) + a_{22}(a_{31}B_x - a_{11}B_z) \\ & \qquad + a_{32}(a_{11}B_y - a_{21}B_x)\} + V_{PH} \\ =& g \,\{a_{13}B_x + a_{23}B_y + a_{33}B_z\} + V_{PH}, \end{aligned}$$

where the offset V_0 was already subtracted and V_{PH} is the voltage due to the planar Hall effect.

In our goniometer method, the terms of B_x, B_y and V_{PH} can be canceled out by a set of measurements with rotations of the goniometer head. The Hall voltages (V_H^0, V_H^{90}, V_H^{180} and V_H^{270}) after rotations of $(\psi + 0°)$, $(\psi + 90°)$, $(\psi + 180°)$ and $(\psi + 270°)$ are written as:

$$V_H^0 = g\,\{a_{13}B_x + a_{23}B_y + a_{33}B_z\} + V_{PH}, \tag{2}$$
$$V_H^{90} = g\,\{a_{23}B_x - a_{13}B_y + a_{33}B_z\} - V_{PH}, \tag{3}$$
$$V_H^{180} = g\,\{-a_{13}B_x - a_{23}B_y + a_{33}B_z\} + V_{PH}, \tag{4}$$
$$V_H^{270} = g\,\{-a_{23}B_x + a_{13}B_y + a_{33}B_z\} - V_{PH}. \tag{5}$$

In all of these measurements (Eqs.2 - 5), the B_z contribution is the same in both sign and magnitude. Thus,

$$\begin{aligned} B_z =& (V_H^0 + V_H^{90} + V_H^{180} + V_H^{270})/4g \cdot a_{33}, \\ \text{and} \qquad V_{PH} =& (V_H^0 - V_H^{90} + V_H^{180} - V_H^{270})/4. \end{aligned}$$

Although $a_{33} = \cos\theta$ (which is ≈ 1 to the first order) has to be determined from a calibration to obtain an exact absolute value of B_z, the way of deducing B_z cancels out the ambiguity of the offset angle of ψ_0 and guarantees the symmetry of the measurement. This is an essential point in a high-precision measurement for the experiment. Similarly, B_x and B_y are obtained.

In the cases where V_{PH} is negligibly small, or it is extracted from a calibration measurement, we may carry out a rationalized method to save time. In this method we run four measurements with (θ, ψ) , $(\theta, \psi + 180°)$, $(\theta + 180°, \psi)$ and $(\theta + 180°, \psi + 180°)$. Here, not only B_z, but also B_x and B_y, can be extracted from the four measurements as:

$$B_x = (V_H^{00} + V_H^{180,180})_x / 2g \cdot a_{33}^x,$$
$$B_y = (V_H^{00} + V_H^{180,0})_y / 2g \cdot a_{33}^y,$$
$$B_z = (V_H^{00} + V_H^{0,180})_z / 2g \cdot a_{33}^z,$$

where $a_{33}^{x,y,z} = \cos\theta_{0x,y,z}$ are the offsets or misalignment $\theta_0 \ll 1$ of each element and the suffix means V_H from the corresponding element. In this measurement symmetry across the median plane is assured. Furthermore, V_0 can be extracted as follows:

$$V_{0z} = (V_H^{00} + V_H^{180,0} + V_H^{0,180} + V_H^{180,180})_z / 4 - \overline{V_{PH}}, \qquad (6)$$

where $\overline{V_{PH}}$ is the mean value of the planar Hall term over all measured points.

3 Field Mapping Device

3.1 3D device

A three-dimensional device (3D device) for field mapping was newly developed (Fig.6a). It is a compact box-type device, very small in size compared to the magnet, and mounted to the magnet gaps with 12 different orientations (Fig.6b). The frame had to have sufficient rigidity for all of these orientations, and should not sag in any direction. The total structure was made entirely using non-magnetic materials. A nest structure was employed to keep a high scanning speed and to make the directional gravitation effect small. The goniometer base plate can move along the z-direction in the z-frame, on three Al slide shafts with a MoS_2 coating with plastic bearings. The z-frame can move along the y-direction in the y-frame on four similar slide shafts. Finally, the x-frame can be moved along the x-direction in the main frame, on four Al shafts with a Ti coating with oil-free metal bushes. All of the movements were driven by pulsed motors using timing belts and pulleys. The goniometer base plate can thus be moved in all three dimensions, and can be located at any point with an accuracy of better than 0.1 mm by means of linear scales of the optical type. The readout accuracy of the linear scales was 10 μm. A continuous feedback of linear scale reading and sending pulses to stepping

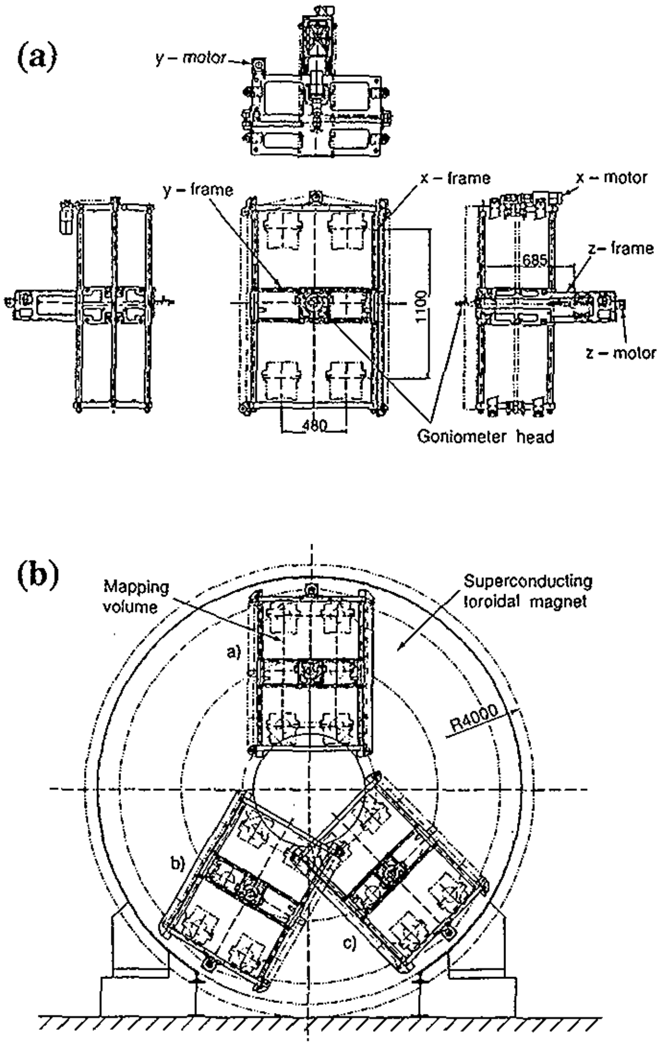

Fig. 6. **3D device:** (a) It is a box type device, very compact compared to the magnet. The total structure was made entirely using non-magnetic materials. A nest structure was employed to achieve high scanning speeds and to make the directional gravitation effect small. The goniometer base plate can move along z-direction in the z-frame. It was mounted to the magnet gaps with 12 different orientations. (b) 3D device mounted on a gap: The installation method was developed by considering the various effects of the gravitation at 12 different orientations.

motors was made to keep the position precisely. The first scanning loop was the z-direction, because the load for the z-drive was smallest and its scanning speed could be much higher than those of other directions. To avoid disturbing the field to be measured, the three motors were located far from the mapping region. Also, linear scales were of the non-magnetic type. For each value of

x, scanning in y- and z-directions was done on the to and from travels of the frames. To reduce the friction of the spline shaft of the y-frame, a spray-type lubricant of MoS_2 was periodically used. The main parameters of the 3D device are listed in Table 1. In this table, the speed does not include the time

Table 1
Main parameters of the 3D device

Attachment angle to the magnet : (30× n) degrees (n=1,12)			
Material : completely non-magnetic			
	x	y	z
Size of frame	1512 mm	1060 mm	580 mm
Range of scanning	1000 mm	480 mm	685 mm
Weight	100 kg	55 kg	4 kg
Driving mechanism			
motor	stepping motor	stepping motor	stepping motor
torque	12kg·cm	17kg·cm	1.4kg·cm
	@ 8.4kpps	@ 6.7kpps	@ 10.5kpps
transmission	timing belts	timing belts	timing belts
		and spline shaft	
slide shaft	4 ×ϕ40 Al rod	4 ×ϕ32 Al rod	3 ×ϕ20 Al rod
	(Ti coated)	(MoS_2 coated)	(MoS_2 coated)
bearing	oil free metal bush	plastics bush	plastics bush
speed	2 mm/s	2 mm/s	9.2 mm/s
positioning precision	0.1 mm	0.1 mm	0.1 mm
Position measurement: non-magnetic optical linear scale			
accuracy: 10 μm			

for the digital volt meter (DVM) reading. It took 2.3 seconds/point on the average to get positioned and to obtain the output voltages by the DVM. The DVM with a GPIB interface had a scanner card, which was connected to 7 outputs from the Hall-probe box. The control system is shown in Fig.7.

3.2 Probe and goniometer head

The Hall probe is shown in Fig.8. Its specifications are listed in Table 2. The Hall-probe temperature was measured with three copper-constantan thermo-

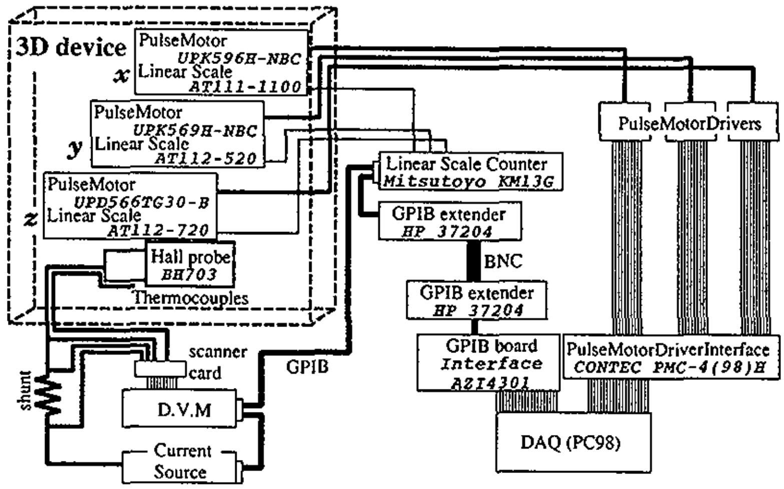

Fig. 7. **Field measurement system:** The DVM had a scanner card which was connected to 7 outputs, $(V_x, V_y, V_z, T_1, T_2, T_3, I_H)$, from the Hall probe box. These data were fed to a data acquisition computer through the GPIB interface together with x, y and z data from the linear scales. A continuous feed-back of linear scale reading and sending pulses to stepping motors was made so as to keep the position precisely. Each frame has edge sensors at both edges connected to the driver interface as interlock switches.

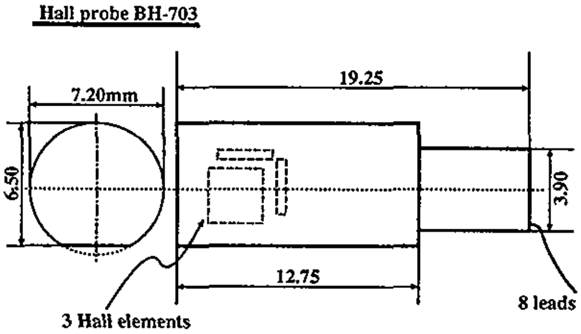

Fig. 8. **Schematic diagram of Hall probe device:** The position and orientation of each Hall element are not seen from outside. The leads consist of $V_x(+,-)$, $V_y(+,-)$, $V_z(+,-)$ and $I_H(+,-)$. The dimensions are in mm.

couples attached to three different points in the small aluminum box. Constantan is an alloy of Ni (40~45%) and Cu (60~55%) and has a very small temperature coefficient of resistance. To prevent any heat leakage, we use a wire having a thickness of 50 μm. Each thermocouple was insulated from the Hall probe with a Mylar sheet. The accuracy of its machining is better than

Table 2
Specification of the Hall probe:BH-703(F.W.BELL)

Zero field residual voltage V_{MT} (B=0),I_c =100mA	100 μV maximum
Angularity	Hall plates, perpendicular within $\pm$ 2°
Control current (a) nominal (b) max continuous	 100 mA 300 mA
Input and output resistance, B=0	3 Ω maximum
Magnetic sensitivity	7.5 mV/kG $\pm$ 20 %
Temperature dependance (a) of Hall voltage (b) of resistance (c) zero field residual voltage	 -0.04%/°C max. +0.15%/°C approx. 0.5μV/°C max.
Operating temperature range	-40°C to +100°C

0.1 mm so that the position of any Hall element can be calculated easily. The box was mounted tightly in the goniometer, which was commercially available and generally used for the optics experiments. The goniometer mounted on the base plate of the 3D device is shown in Fig.9, the head of the goniometer could be oriented to any direction. The goniometer was made entirely from aluminum according to a special order to avoid distorting the magnetic flux. The Hall-probe housing is shown in Fig.10, and the parameters of the goniometer system are summarized in Table 3.

Table 3
Main parameters of the goniometer system

Range of rotation	$\phi = 0° - 360°$ $\theta = 0° - 360°$ $\psi = 0° - 360°$
Accuracy of setting (reading accuracy)	$\Delta\phi = \Delta\psi = 0.1°$ $\Delta\theta = 4 \times 10^{-4}$rad (by micrometer)
Inner diameter of the holder	D = 30 mm ϕ
Height of rotation center from the base plate	H = 160 mm
Material	Al

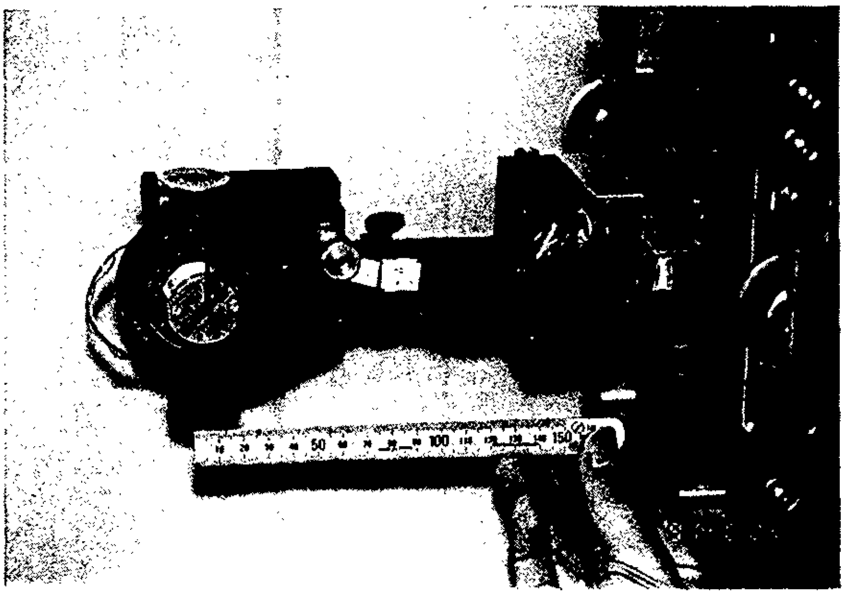

Fig. 9. **Goniometer mounted on a 3D device:**

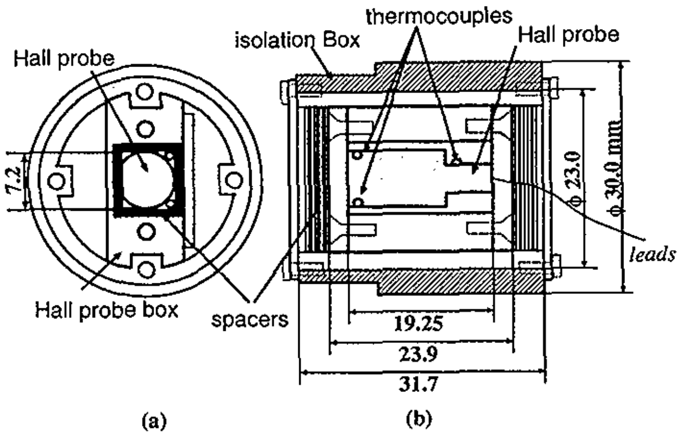

Fig. 10. **(a) Cross section of the Hall-probe housing:** The Hall probe was fixed tightly and adjusted with some 0.1 mm-thick spacers both vertically and horizontally. Each thermocouple was insulated from the Hall probe with a Mylar sheet. **(b) Top view of Hall probe housing:** Hall-probe box position along the central axis of the isolation box was adjusted with spacers with an accuracy of 0.1 mm. Plastic screws were used.

The 3D device was mounted to the exit of each magnet gap of the toroidal spectrometer with an aluminum base plate for fine alignment (Fig.11). Before

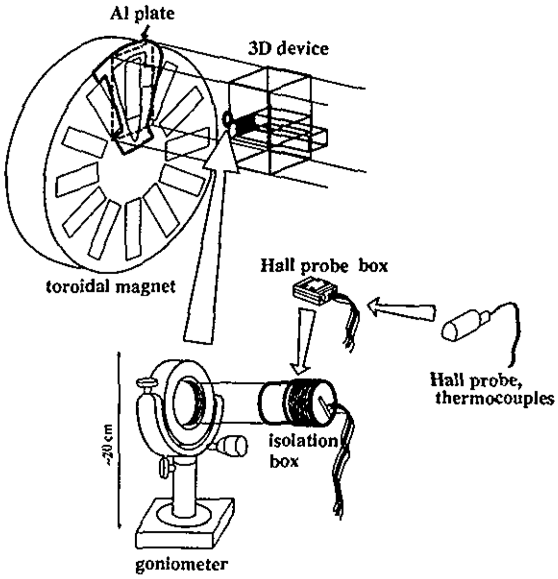

Fig. 11. **Setup of field measurement:** An aluminum plate (shadowed part) for fine alignment was installed between Toroidal Spectrometer and the 3D device. Relative positions can be calculated with an accuracy of 0.1 mm. All parts were made of non-magnetic material.

starting the field measurement, the position adjustment was done carefully. The distortion of the 3D device, itself, was corrected by a laser-positioning system after a fine alignment. The scheme of the laser-beam alignment is shown in Fig.12. The system was located on the median plane of each sector. By using the two collimators with a 0.5 mm diameter and a thickness of 6.0 mm 80 cm apart, the laser beam was completely parallel to the reference z-axis of the toroidal spectrometer. The beam was detected by a phototransistor (TS604-3F, TOSHIBA) just behind the third collimator with a diameter of 1.0 mm. The phototransistor and the third collimator were fixed accurately on the goniometer base plate. The output voltage of the phototransistor was measured by DVM. The phototransistor and the third collimator system were scanned in the x- and y-directions over about 1 cm in 9 scanning areas. Measurements were made at 3 points on each axis of A-A, B-B and C-C shown in Fig.12. The maximum distance along the z-direction was 670 mm. In this way, not only the spacial offset of the 3D device, but also its distortion due to gravity, were obtained.

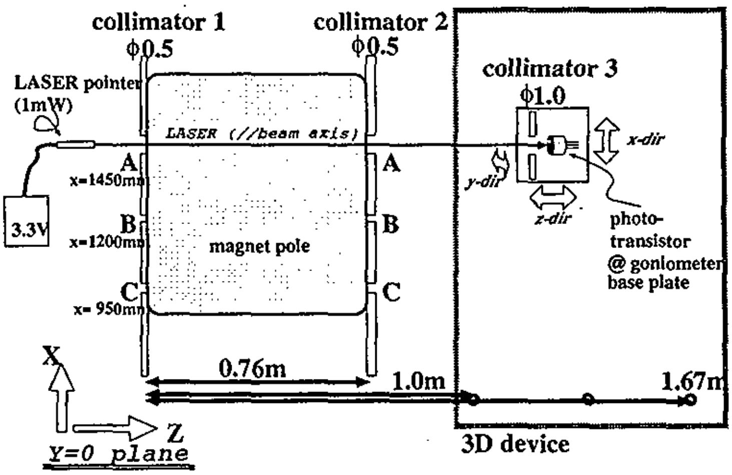

Fig. 12. **Schematic view of the laser positioning system:** The system was located on the median plane of each sector. The laser beam was parallel to the reference z-axis. The beam was detected by a phototransistor just behind the collimator 3. Measurements were made at 3 points on each axis of A-A, B-B and C-C.

The typical spectra of the output voltage of the phototransistor is shown in Fig.13. The side peaks are due to the Fraunhoffer diffraction. The observed peak position were not affected by a small displacement of the laser pointer light source. The laser system has an accuracy of about 0.1 mm after fitting. Good reproducibility of the peak position could be confirmed even after repeated mounting and dismounting of the collimators. Regarding the z-direction, the reference position was defined by touching the edge of the spectrometer shim plates with a positioning pin.

In order to simplify the angular relation between the Hall elements and the 3D device, the orientation of the goniometer head, including the Hall probe, was fixed so that the normal vector of the y-element was completely parallel to the y-axis of the 3D device. The last remaining ambiguity of the angle around the y-axis was removed by setting so that the normal vector of z-element lies completely in the y-z plane of the 3D device. In this condition, the z-normal vector must be the nearest to the z-axis.

4 Hall Probe Calibration

Before the measurement, the following Hall-probe calibrations were performed: (1) determination of temperature coefficient, (2) determination of the position of three Hall elements in the Hall-probe mould with an accuracy of $\sim$ 0.1 mm,

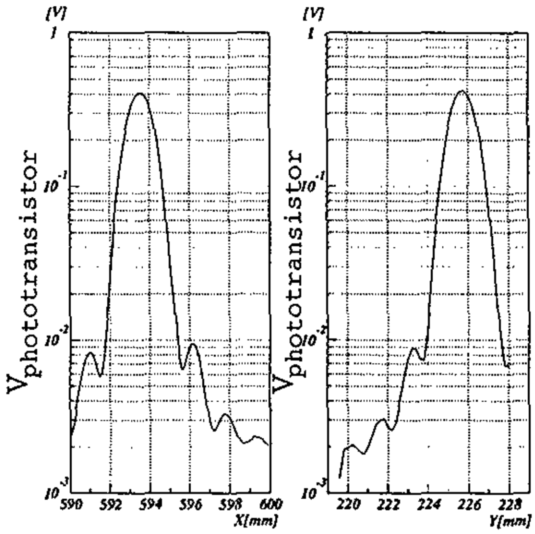

Fig. 13. **Typical spectra of the output voltage of the phototransistor as a function of the X,Y position:** The peak point and its width were obtained by fitting with an accuracy of 0.1 mm. The side peaks are due to the Fraunhoffer diffraction.

(3) determination of the orientation of each Hall element in the mould with an accuracy of $\sim$ 0.2 degree, and (4) the V_H - B calibration.

4.1 Temperature Dependence

A measurement of the temperature coefficient of V_H was carried out using a permanent dipole magnet with a 1.2 kGauss of field in a 15 cm gap between 40 cm $\times$ 30 cm pole faces. The setup is shown in Fig.14. In the Hall-probe box, the Hall probe and three thermocouples were fixed tightly to the base plate of the box. The supplied current to the Hall probe was 100 mA, the same as in a real measurement. The instability of the current caused fluctuations of V_H, a source of error in the measurement. A shunt register of 1.0 Ω was used as a current monitor for the correction of V_H. Generally, a thermocouple needs a reference temperature, e.g., 0°C. In this measurement, however, three compensators were used to provide the reference temperature electrically.

The temperature of the probe was not controlled, but just followed the ambient temperature. The measurement was performed for about 45 hours. The average measurement time for one point is 11 seconds. In order to avoid any rapid changes in the temperature, the volume in the gap was covered with an isolating material.

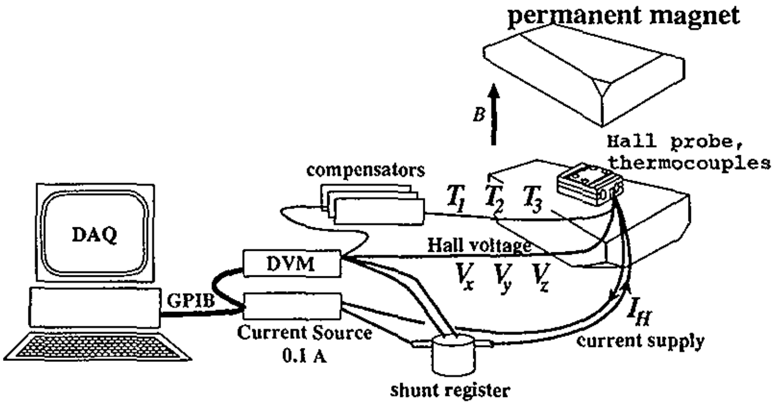

Fig. 14. **Setup of the temperature-dependence measurement:** The permanent dipole magnet had a field of 1.2 kGauss in the 15 cm gap. A shunt register of 1.0 Ω was used as a current monitor. The three compensators were used to provide the reference temperature electrically. The DVM had a scanner card connected to 7 outputs (V_x, V_y, V_z, T_1, T_2, T_3 and I_H).

The V_H decreases with temperature, as shown in Fig.15. From this plot, temperature coefficient was extracted to be about -0.031%/°C in good agreement with the manufacture's specification. The accuracy of temperature measurement is about ±0.3 °C, and this spread of point is due to the current instability.

4.2 Hall Element Position Calibration

Three Hall elements were embedded in a monolithic mould, as shown in Fig.8, and the position of the element could not be seen from outside. The position had to be fixed with respect to the Hall probe box. To do this calibration, the setup of permanent magnets with two iron pins, which generated a very sharp and narrow field shape, was used (Fig.16). We used 8 pieces of 12.1 kGauss permanent magnets of NEOMAX-35 of $Nd_2Fe_{14}B$ with a dimension of $10 \times 5 \times 3$ mm^3. The Hall-probe box was scanned around the pins where the field was enlarged. About 50 points were measured. The V_H was monitored and had the maximum value when the element was just above the apex of the cone. Fig.17a is a plot of V_H of the normal element as a function of horizontal (y, z) position shown in Fig.16(a). The maximum field strength was about 4.5 kGauss, approximately in the mid-plane of the two pins. After the fitting by spline curves of a convexity, as shown in Fig.17b, the peak position, which could be identified as the center of the element, was obtained with an accuracy of better than 0.1 mm. The principal source of error was in reading the scale of the scanning system. The height of the element was extracted from the

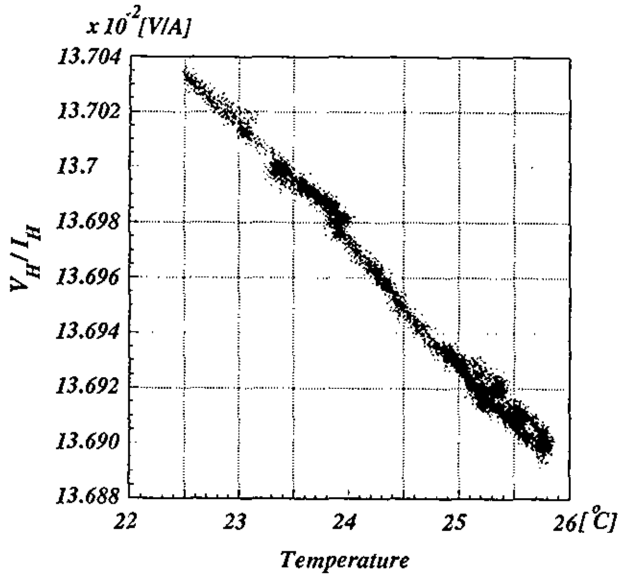

Fig. 15. **Temperature dependence of the Hall coefficient (V_H/I_H) as a function of the temperature**: The temperature coefficient was extracted to be $-0.031\%/°C$. This has a good agreement with the specification.

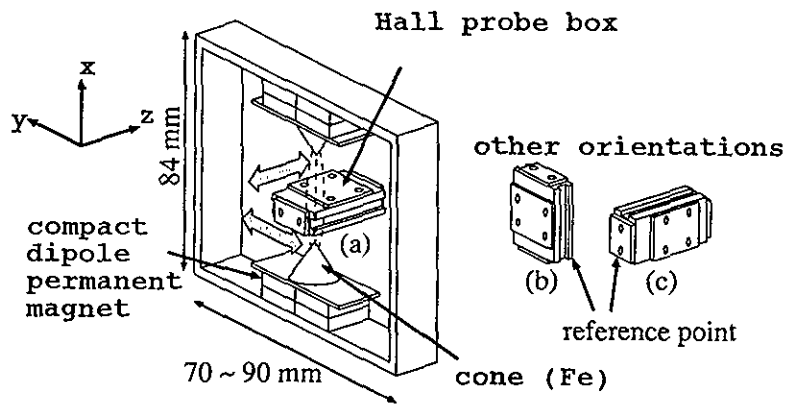

Fig. 16. **Setup for fixing the position of each element**: The Hall-probe box can move along the two directions (shaded arrows) in a small permanent-magnet frame. Eight pieces of 12.1 kGauss permanent magnets of NEOMAX-35 of $Nd_2Fe_{14}B$ with a dimension of $10 \times 5 \times 3$ mm^3 were used as a source of flux. Two iron cones (pins) generated a very sharp field shape. In order to obtain the element position, the measurement was carried out in three different box orientations.

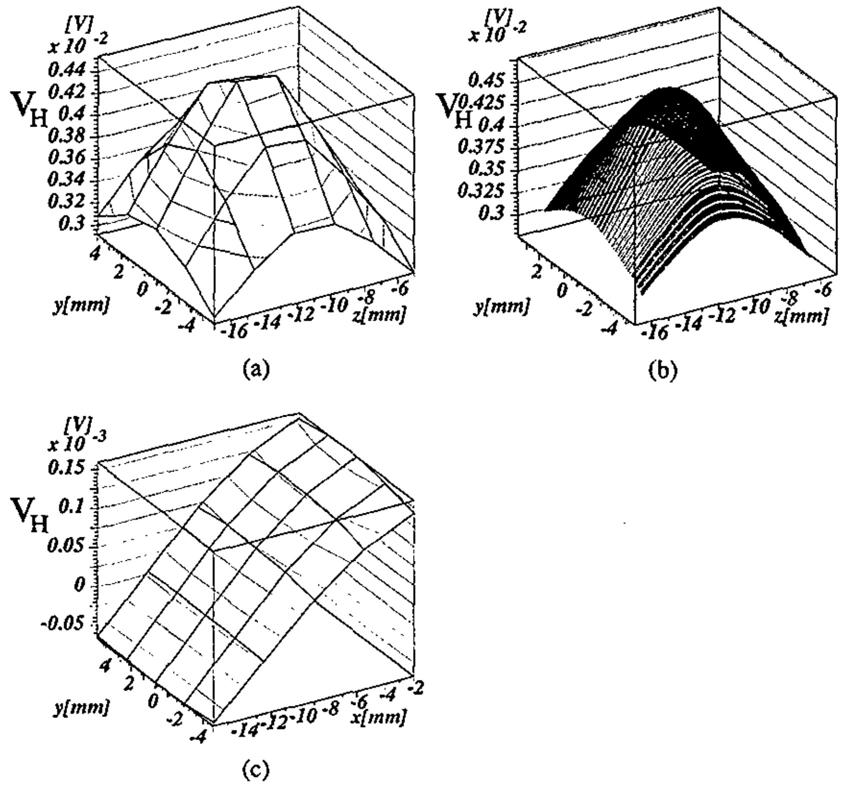

Fig. 17. (a) V_H as a function of the horizontal position(raw data). (b) V_H as a function of the horizontal position(fit by spline curve): The field strength at the maximum was about 4.5 kGauss on the approximately mid-plane of the two pins. (c) V_H as a function of the horizontal and vertical position: V_H did not show a peak, but has a slope crossing zero as a function of the horizontal position. The center of the element was identified as the peak in (b) and the height on the zero-crossing point.

zero-crossing point corrected for V_0 in the x, y scan (Fig.17c). In this case, the orientation of the Hall-probe box of Fig.16(b) was used. In order to obtain the position of all three elements, the measurement was carried out in three different box orientations (Fig.16). The positions obtained and corrected by the offset values are listed in Table 4.

4.3 Hall-voltage calibration and Determination of the Hall-plane angles

In a small magnetic field, the planar Hall effect is very small compared to the normal Hall effect. For the E246 experiment also, the relevant field in the polarimeter is less than 300 Gauss, and, thus, the normal Hall effect dominates.

Table 4
Position of each element in the mould

Element	Relative position [mm]	Error
X	(4.6, 3.5, 10.3)	0.1
Y	(5.2, 3.6, 9.9)	0.1
Z	(4.0, 1.2, 9.0)	0.1
ref. point	(0.0, 0.0, 0.0)	

However, through an analysis of the planar effect, angular corrections can be determined. [3–6].

There may be misalignments of the Hall-element orientation. According to the specification, this angular ambiguity should be less than 2°. In order to obtain the exact angle of each Hall element, a calibration measurement was made using a sufficiently homogeneous field of 1.0 T, which was generated by a H-type magnet. In this calibration, not only the angle information, but also V_0 and the Hall coefficients, were obtained.

With the goniometer, the Hall probe can be rotated in any direction in the magnet gap. The three output voltages (V_x,V_y and V_z) were recorded for any possible combination of three angles (ϕ, θ, ψ).

The field strength (B) was monitored by an NMR probe. V_z is, for example, expressed as

$$\begin{aligned} V_z = & V_0 + GB\cos(\theta + \theta_0) \\ & + PB^2 \sin^2(\theta + \theta_0) \sin 2(\psi + \psi_0) \end{aligned}$$

using the definition in Fig.4. Fig.18 shows the output voltages of the Hall probe. When ϕ and ψ were fixed, the normal Hall effect was seen as a function of θ (Fig.18a). The four regions of θ where V_H's have maximum, minimum and zero-cross were measured in fine step. The planar term was obtained as a function of ψ (Fig.18c), under the condition of ($\phi = 0$, $\theta + \theta_0 = 90°$). The output voltage in the condition that planar Hall effect dominated was decomposed to each effect by fitting as shown in Fig.18c. A sine curve with a period of 180° corresponds to the planar effect. Another sine curve shows the normal Hall effect. During a measurement in which the three angles (ϕ, θ, ψ) varied individually, not only V_z, but also V_x and V_y, were recorded. For the z-element, for example, the Eulerian angles of $\vec{n}_z$, $\vec{I}_{Hz}$ and three Hall effect parameters were obtained for a field of 100 Gauss by fitting of about 40 points to be:

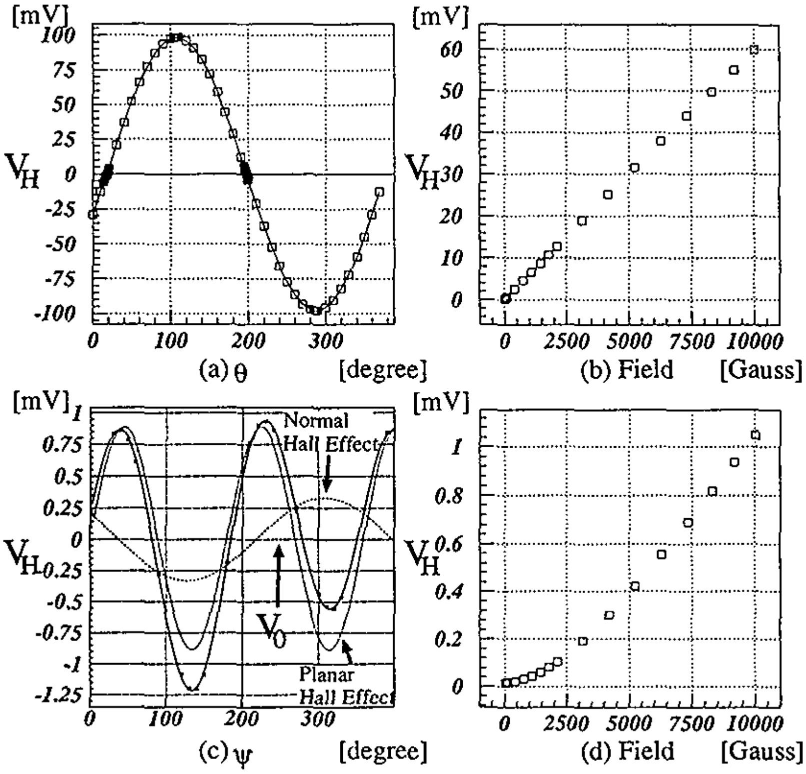

Fig. 18. **Output voltage of the Hall probe as a function of θ, ϕ and field magnitude:** (a) The normal Hall effect as a function of θ (b) The linearity of the normal Hall voltage to the field. The Hall element had an angle of $\cos\theta = 0.6$. (c) A typical planar Hall effect was extracted from the decomposition of the voltage to the normal Hall effect, V_0 and the planar Hall voltage. Symbols correspond to the measured points. The sine curve with the period of 180° corresponds to the planar effect. Another sine curve shows normal Hall effect. The offset voltage V_0 ($= -3.49\ \mu$V) is overlapped by the grid line of $V_H = 0$. (d) The relation of the amplitude of the planar Hall effect to the field.

$$\vec{n}_z = A(\phi_0 = 1.0°, \theta_0 = 197.5°) \begin{pmatrix} 0 \\ 0 \\ 1 \end{pmatrix},$$

$$\vec{I}_{Hz} = A(\phi_0 = 1.0°, \theta_0 = 197.5°, \psi_0 = -71.9°) \cdot I \begin{pmatrix} 1 \\ 0 \\ 0 \end{pmatrix},$$

$$V_{0z} = -3.49 \pm 0.01\mu\text{V}, \qquad G_z = (9.5042 \pm 0.00019)\mu\text{V/Gauss},$$
$$P_z = (8.5662 \pm 0.0570) \times 10^{-6}\mu\text{V/Gauss}^2,$$

where ϕ_0, θ_0 and ψ_0 are offset angles of the goniometer including misalignment. Fig.18b shows a linearity of the normal Hall effect. It was found that there was sufficiently small fluctuation compared with that of the NMR monitor. In this plot, the Hall element had an angle of $\cos\theta$=0.6. Fig.18d shows the field dependence of planar Hall effect, PB^2. V_0 and GB at 100 Gauss for each element were obtained with an error of 2 μV. Also, the misalignment in angle was detected to be $\sim 1°$ with an error of 0.2°. The error was mainly due to reading the scale of the goniometer. The results for the x- and y-elements were similar.

5 Measurement and Analysis

Measurements were made for all 12 sectors. As a reproducibility test, the measurements for one sector were repeated, and the results were satisfactory. The measured region was: ($0 \leq x \leq 1000$ mm, $0 \leq y \leq 480$ mm, $0 \leq z \leq 685$ mm), as shown in Fig.6a. It covers the stopper region completely and has an overlap with an adjacent magnet sector.

In the mapping, the following 10 data were recorded through GPIB into a computer $(x, y, z, V_x, V_y, V_z, T_1, T_2, T_3, I_H)$. Here, x, y and z are the coordinates of the position supplied by linear scale controllers as digital signals; V_x, V_y and V_z are the output voltages from the three elements. T_1, T_2 and T_3 are the temperatures of Hall probe monitored by three thermocouples in the box. The temperature of the probe was not controlled, but followed the ambient temperature of the room, whose temperature was stabilized to $\pm$ 1°. The average of three temperatures was used as the Hall-probe temperature. I_H is a Hall current of 100 mA. The stability of I_H was monitored by a shunt voltage recorded with a DVM. The raw data of V_x, V_y and V_z were divided by I_H and then corrected for any temperature change and offset by V_0, giving final data of V_{x3}, V_{y3} and V_{z3}.

An NMR probe continuously monitored the field magnitude at the center of magnet gap. The toroidal spectrometer has no significant hysteresis and good field reproducibility of better than 10^{-5} between the supplied current and the field magnitude.

Several measurements were performed, as listed in Table 5. For the purposes of calibrations, the measurements by method (A) were optimized in order to determine the matrix elements, a_{ij} $(i, j = 1, 3)$, in an effective way. The measurement was done in the 4 conditions of ($\theta + \theta_0$, $\psi + \psi_0$)= (0°, 0°), (0°, 180°), (180°, 0°) and (180°, 180°). As was discussed in section 2, the combination of two sets of measurements out of four V_H's could cancel two other uninteresting components and the symmetry of the measurement was

Table 5
Types of measurements

Method	purpose or comments	x-region [mm]	y-region [mm]	z-region [mm]	step [mm]	time [hour]
(A)	goniometer head rotation and check of calibration	400	160	620	40	10
(B)	mapping	660	180	300	20	9
(C)	overlap region with adjacent sectors	225	50	400	50	2
(D)	the region where muon stop distribution is dense	const.	185	620	10	2
(E)	the region where field gradient large	700	185	const.	10	6
(F)	x-outer edge	const.	185	620	10	2

confirmed. At the same time, the fluctuation of V_0 was checked. Except for method (A), the goniometer head angles were fixed accurately and tightly, as described in the following. For the practical reason of the mapping time, a real field map was constructed by method (B), which covers the muon stopper region. Method (C) was used for a test of the continuity with an adjacent sector in the overlap region. The region of (D) was included in (B), but had a fine step size. In this region, the muon stop position distribution in the muon stopper is dense according to a Monte-Carlo simulation. The region where the field gradient is large was measured with a fine step by the menu (E). Method (F) was used for testing the field symmetry in a large x-region. In a region far from the yokes and the shims, the field symmetry might be affected by magnetized material, e.g., the support and jig of the spectrometer and refrigerator system. All menus were done within a few days per gap.

For the measurements (B), (C) and (D), the field components were extracted as follows. When the 3D device is perfectly aligned to the toroidal magnet as was described in section 3.3, B_y is just V_{y3} multiplied by G_y. To see this, let us suppose that α is the angle between $\vec{B}_{yz}$ and y-axis, as shown in Fig.19, where $\vec{B}_{yz}$ is a projected field vector to y-z plane.

$$\frac{B_z}{B_y} = \tan\alpha,$$

$$B_{yz} = \sqrt{B_y^2 + B_z^2}.$$

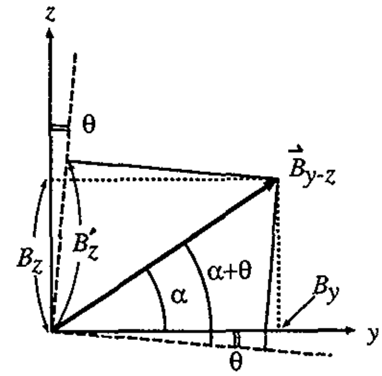

Fig. 19. **Field vector projected to y-z plane:** α is the angle between $\vec{B}_{yz}$ and y-axis, $\vec{B}_{yz}$ is the projected field vector to y-z plane. B_z is the real z-component to be determined. B'_z is the measured z-component. θ is the calibrated mis-alignment angle of z-element with respect to the z-axis.

With the measured z-component, B'_z,

$$B'_z = B_{yz}\sin(\alpha+\theta),$$

where θ is the calibrated misalignment angle of z-element respect to z-axis. From above equations, α can be written in terms of $(R,\ \theta)$, as follows:

$$\tan\alpha = \frac{R-\sin\theta}{\cos\theta}, \qquad \text{where} \qquad R \equiv \frac{B'_z}{B_y} = \frac{\sin(\alpha+\theta)}{\cos\alpha}.$$

Therefore, the field components B_y and B_z are expressed by:

$$B_y = G_y \cdot V_{y3},$$
$$B_z = \left(\frac{G_y \cdot V_{z3}}{B_y} - \sin\theta\right) \cdot \frac{B_y}{\cos\theta}.$$

For B_x, another plane, γ, was introduced analogous to that of B_z, as seen in Fig.20. $\vec{B}'_x$ is the measured x-component direction, that is, the normal vector of x-element. Unlike B'_z, $\vec{B}'_x$ is not always on γ plane but has misalignment angles $\varepsilon_1 \approx 1°$ and ε_2 in polar and azimuthal angles. ϕ' defined as the angle of $\vec{B}'_x$ with respect to $\vec{B}_{yz}$ is fixed by ε_1, ε_2 and α. Then, $\vec{B}''_x$ is introduced with a misalignment angle (ϕ) of $90° - \phi'$, and B''_x can be regarded as B'_x, because the difference $(B''_x - B'_x)/B'_x$ is less than 10^{-4} for $\varepsilon_1 \approx 1°$. The difference is

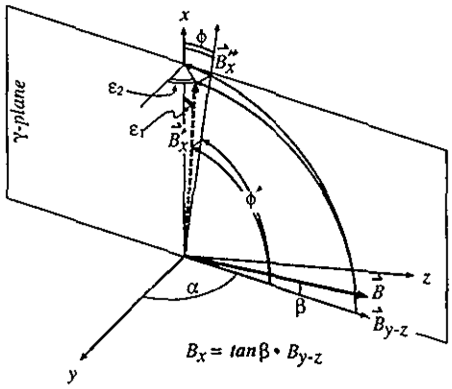

Fig. 20. **Plane introduced to extract the B_x component**: the γ-plane includes the x-axis and $\vec{B}$. $\vec{B'_x}$ is not always on the γ plane, but has mis-alignment angles (ε_1) of $\approx 1°$ and ε_2 in polar and azimuthal angles. ϕ' defined as the angle of $\vec{B'_x}$ with respect to $\vec{B_{yz}}$ is fixed by ε_1, ε_2 and α. $\vec{B''_x}$ is introduced with a misalignment angle (ϕ) of $90° - \phi'$, and B''_x can be regarded as B'_x because the difference $(B''_x - B'_x)/B'_x$ is less than 10^{-4} for $\varepsilon_1 \sim 1°$.

negligible for our case of $B_x/\sqrt{B_y^2 + B_z^2} < 10^{-2}$. As $B_x = \tan\beta \cdot B_{yz}$, B_x is expressed as

$$B_x = \left(\frac{G_x \cdot V_{x3}}{B_{yz}} - \sin\phi \right) \cdot \frac{B_{yz}}{\cos\phi}.$$

The second-order terms of B_x, B_y and B_z, from the planar Hall effect, can be neglected, because the field strength is less than 300 Gauss and the normal Hall effect is dominant. In an actual measurement, there was a misalignment of the 3D device with respect to the toroidal magnet. This misalignment could be detected by the laser-positioning system. And this was corrected by a small rotation of the 3D device due to a tilt or distortion. The correction was the transformation from the measured orthogonal coordinate to the real orthogonal one. The order of matrices of the rotations was not important, because the rotation is very small.

The analysis was done with the corrections affected for; (1) temperature dependence, (2) orientation and position of each Hall element, (3) self-distortion of 3D device. And finally self-consistency was checked by some data set described in Table 5.

Fig.21 shows the self-distortion of the 3D device when it was mounted at one sector. Δx in Fig.21a is the shift along the x-direction, which was measured by the laser-positioning system. With the help of fits of the Fig.13 data, it

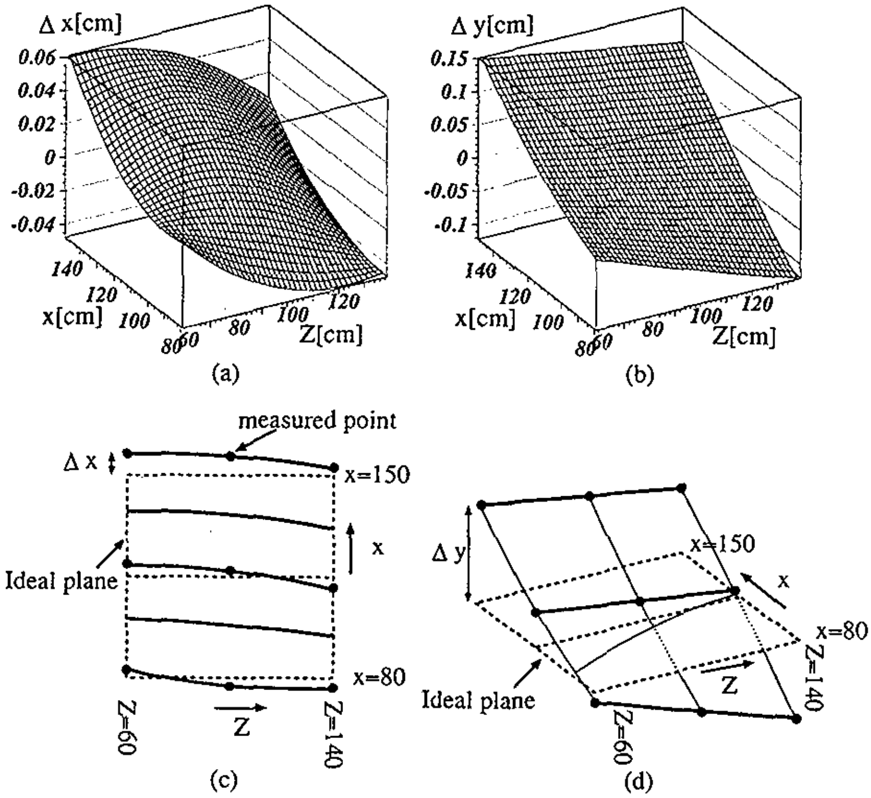

Fig. 21. **(a) Δx of a distorted plane:** Δx is a shift along x-direction which was measured by the LASER positioning system. **(b) Δy of distorted plane** (c) and (d) depict the distorted shape of a 3D device with solid lines. The ideal planes are expressed by dotted lines. Interpolation used curves of the second-order.

was possible to determine Δx to a precision of better than 0.1 mm. Fig.21c shows the distorted shape of the 3D device as solid lines. The ideal plane is expressed by dotted lines. Δy in Fig.21b means a shift in y-direction. Fig.21d is a schematic explanation. From Fig.21d, it was found that Δy was due to a tilt by a small rotation of the 3D device. This kind of deformation is different from gap to gap. Thus, an analysis was carried out for all 12 gaps. With the data set for all sectors, the transformation from linear scale reading to the real position for any point was obtained. Interpolation by a second-order polynomial was used to determine the positions and fields as the points that were not measured. Table 6 summarizes the positioning precision of each component, and also the methods employed to attain them. The accuracy of relative position of Hall element to the goniometer base plate was calculated to be 0.2 mm. For the goniometer base plate and the toroidal magnet, its accuracy is better than 0.2 mm. The resolution corresponds to an accuracy in orientation on the

Table 6
Position accuracy of each part

relation	accuracy	method
Hall element position – probe box	0.1 mm	fitting
probe box – isolation box	0.1 mm	machining
isolation box – goniometer	0.1 mm	machining
goniometer – base plate on 3D device	0.1 mm	machining
Hall element – base plate	0.2 mm	
collimator3 – base plate (x, y)	0.1 mm	machining
collimator3 – laser beam (x, y)	0.1 mm	fitting
laser beam – magnet*	0.1 mm	machining
base plate – magnet (z)	0.05 mm	gap gauge
base plate – 3D device	0.01 mm	linear scale
base plate – magnet	< 0.2 mm	

*The accuracy of laser beam is given for the muon stopper region.

order of 10^{-3} rad for a typical distance of 300 mm in the laser positioning.

As mentioned in section 2, V_0 of each Hall element was obtained by rotating of the goniometer head at all measured points using Eq.(6). This means that V_0 was measured at about 600 points in one sector. Fig.22 shows the average (root mean square) V_0 of the z-element versus the sector number. Over all sectors, V_0 was almost constant and had small fluctuation of about 1 μV, which corresponds to 0.1 Gauss. In a field of 100 Gauss, the error of V_0 is dominant compared to that of GB, and $\overline{V_{PH}}$ is the level of 10^{-5} relative to the field strength. It corresponds to the order of 0.01 μV. Thus, from Fig.22, it was found that measurements of the voltage were carried out precisely enough with a precision of 0.1 Gauss (root-mean square of each gap is 0.07 Gauss). A measurement scanning more points would give a smaller error. This could induce the error of the order of 10^{-3} rad in the orientation of a field vector of 100 Gauss. Fig.23 describes the magnitude of the polarimeter field in the median plane of a sector. The rectangle corresponds to the muon stopper region. The muon stopper is covered with a field of 120 Gauss on the average. Taking into account the muon stop distribution, almost all muons stop in a field of more than 100 Gauss.

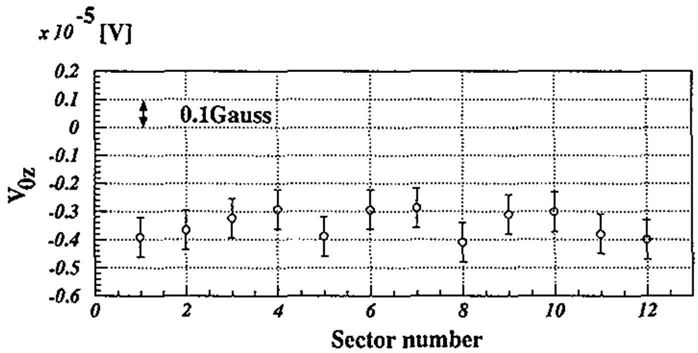

Fig. 22. V_{0z} **vs. sector number**: The error bars correspond to the root-mean square. Over all sectors, V_0 was almost constant and had a small fluctuation of about 1 μV, which corresponds to 0.1 Gauss. For each gap, the root-mean square value is 0.07 Gauss, which could be regarded as the accuracy of the measurement. These V_0 have good consistency with the calibration value of -3.49 μV.

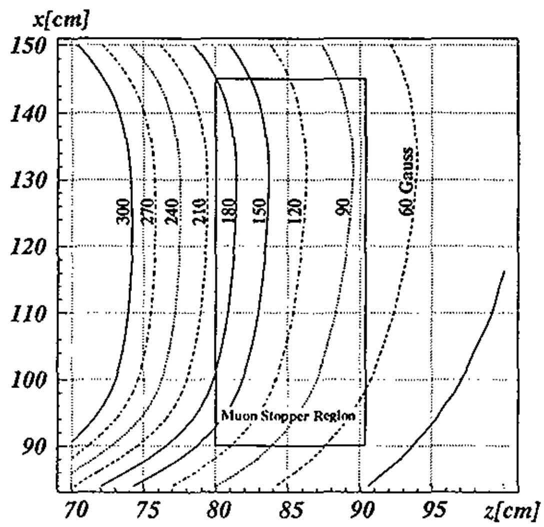

Fig. 23. **Field magnitude on y=0 plane**: The rectangle corresponds to the muon stopper region. The muon stopper is covered with a field of 120 Gauss on the average. Taking into account the muon stop distribution, almost all muons stop in a field of more than 100 Gauss.

6 Conclusions

Inhomogeneous magnetic field mapping in a polarimeter for a T-violation experiment using $K_{\mu 3}$ decay was carried out precisely with new techniques using a 3D Hall probe and a goniometer which are now commercially available. In the polarimeter the symmetry of the field distribution across the median plane is essential as long as the muon-stopping distribution is assured. (1) High-precision positioning of a measured point, (2) mechanism to guarantee the symmetry with respect to the median plane, (3) accurate measurement of the three field components and (4) high-speed operation were required for the field mapping. To satisfy these requirements, a 3D Hall-probe method was employed, because of its compactness and time saving. Problems in using a 3D probe were overcome by (1) the goniometer method, (2) high-performance 3D device, (3) accurate temperature monitor and (4) careful calibration of the orientations and positions of the Hall elements in the 3D probe. Using the developed goniometer system, the 3D Hall probe which was mounted on the goniometer head could be rotated to any direction around three orthogonal axes. The method has not only the easiness of angular adjustment, but also provides us with the ability to extract the normal Hall effect, eliminating the influence of the planar Hall term, and a rationalized mapping which guarantees exact symmetry of the measurement under the condition of a small Hall planar effect. The 3D device was developed for a scanning system with a high-precision position measurement. No significant problem due to the gravitation occurred at any gap of 12 different orientations. Combined with the laser positioning system, not only the spacial offset of the 3D device, but also its distortion, was obtained. The automatic computer control and the small load for z-drive allowed us a high speed mapping. As the Hall probe calibration, the temperature coefficient, the position of three Hall elements in the mould, the orientation of these elements and the relation of V_H to field were determined. The temperature coefficient was determined in a separate measurement using a permanent dipole magnet. The position of these elements were fixed with a sharp and narrow field of 4.5 kGauss induced by iron pins. The orientation and the relation of V_H to field were determined by rotation of the goniometer head in a homogeneous field of 1.0 T and then fitting with a function including the planar Hall effect. In the measurement, several types of methods were performed. For a confirmation, V_0 was extracted from the measurement by flipping the goniometer head. It was found that the V_0 had a small fluctuation corresponding to 0.07 Gauss for one gap and was constant over 12 gaps. V_0 was consistent with the calibrated V_0 value. Total accuracies of <0.5 mm in position, 0.07 Gauss in field and 10^{-3} rad in angle were obtained. The field map made by the filed measurement has been analyzed and is being used in an analysis of the experiment.

Acknowledgement

The authors are thankful to the other members of the E246 collaboration for valuable discussions.

References

[1] J.Imazato, *et al.*, KEK Report 91-8, 1991.
[2] J.Imazato, *et al.*, KEK Preprint 96-161, 1997.
[3] B.Turck, *et al.*, Nucl. Instr. and Meth. **95**, 205 (1971).
[4] K.Amako, *et al.*, Nucl. Instr. and Meth. **197**, 325 (1982).
[5] H.Kichimi, *et al.*, Nucl. Instr. and Meth. **A251**, 469 (1986).
[6] T.Hasegawa, Doctor thesis, University of Tokyo, INS-IM-15, (1994).